

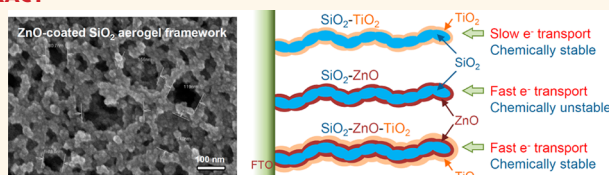
Fast Transporting ZnO–TiO₂ Coaxial Photoanodes for Dye-Sensitized Solar Cells Based on ALD-Modified SiO₂ Aerogel Frameworks

Venessa O. Williams,[†] Nak Cheon Jeong,[†] Chaiya Prasittichai,[†] Omar K. Farha,[†] Michael J. Pellin,^{†,‡} and Joseph T. Hupp^{†,*,§}

[†]Department of Chemistry and Argon-Northwestern Solar Energy Research Center (ANSER), Northwestern University, 2145 Sheridan Road, Evanston, Illinois 60208, United States, [‡]Materials Science Division, Argonne National Laboratory, 9700 S. Cass Avenue, Argonne, Illinois 60439, United States, and [§]Chemical Science and Engineering Division, Argonne National Laboratory, 9700 S. Cass Avenue, Argonne, Illinois 60439, United States

Among the most efficient classes of excitonic photovoltaic devices are dye-sensitized solar cells (DSSCs),^{1–6} especially those modeled after the design pioneered by O'Regan and Grätzel in 1991.⁷ The most ubiquitous versions of DSSCs harness high-surface-area, sintered nanoparticle networks (*ca.* 1000× geometric area or greater) loaded with modified ruthenium polypyridyl complexes to harvest light with good efficiency across all but the red-most portion of the visible spectrum. Additionally, they are characterized by reasonably efficient electron injection (*i.e.*, excited dye to semiconductor injection) and highly efficient electron collection, at least when iodide/tri-iodide (I^-/I_3^-) is used as the redox shuttle.⁸ Despite these attributes, the highest energy conversion efficiencies are *ca.* 12.3%,⁹ about a third of the theoretical limit of 32% for a single junction cell in the absence of special mechanisms such as carrier multiplication. We and others have noted that the single greatest source of energy loss in most high-performance DSSCs is in the regeneration of the chromophoric form of the dye *via* reduction with iodide.^{3–5,10,11} In order to accomplish regeneration at a suitable rate (*i.e.*, significantly faster than the rate of return of the injected electron to the oxidized dye), a driving force of close to 600 meV is required. To appreciate how significant this loss is, note that champion cells operating at the peak power point generate photovoltages of slightly less than 800 mV. All else being equal, if the driving force for dye regeneration could be decreased to, say, 200 meV, and if the gains were folded into the photovoltage, the DSSC energy conversion efficiency would

ABSTRACT



A doubly coaxial photoanode architecture based on templated SiO₂ aerogels was fabricated on transparent conducting oxides for use in dye-sensitized solar cells (DSSCs). These templates were coated with ZnO *via* atomic layer deposition (ALD) to yield an electronically interconnected, low-density, high-surface-area, semiconductor framework. Addition of a thin conformal layer of a second metal oxide (alumina, zirconia, or titania) *via* ALD was found to suppress the dissolution of ZnO that otherwise occurs when it is soaked in alcohol solutions containing acidic dyes used for sensitization or in acetonitrile solutions containing a pyridine derivative and the iodide/tri-iodide (I^-/I_3^-) redox shuttle. Electron transport in SiO₂–ZnO–TiO₂ photoelectrodes was found to be nearly 2 orders of magnitude faster than in SiO₂–TiO₂ structures, implying that the interior ZnO sheath serves as the primary electron conduit. In contrast, rates of electron interception by the oxidized form of the redox shuttle were observed to decrease when a TiO₂ shell was added to SiO₂–ZnO, with the decreases becoming more significant as the thickness of the titania shell increases. These effects lead to improvements in efficiency for DSSCs that utilize I^-/I_3^- , but much larger improvements for DSSCs utilizing ferrocene/ferrocenium, a notoriously fast redox shuttle. For the former, overall energy conversion efficiencies maximize at 4.0%. From a variety of experiments, the primary factor limiting aerogel-based DSSC performance is light loss due to scattering. Nevertheless, variants of the doubly coaxial structure may prove useful in devising DSSCs that can achieve excellent energy conversion efficiencies even with fast redox shuttles.

KEYWORDS: dye-sensitized solar cell · atomic layer deposition · zinc oxide · aerogel · ferrocene redox shuttle

increase to nearly 16%. Alternatively, if the gains were deployed to make feasible the use of a dye absorbing an additional 0.4 eV to the red, more photons would be captured, more current would be generated, and the DSSC energy conversion efficiency would reach about 18%.¹⁰

With these and other considerations in mind, there has been a renewed and

* Address correspondence to j-hupp@northwestern.edu.

Received for review April 9, 2012 and accepted June 21, 2012.

Published online June 21, 2012 10.1021/nn3015695

© 2012 American Chemical Society

expanded focus on alternatives to iodide/tri-iodide as the standard redox shuttle.^{12–24} (Tri-iodide has other drawbacks, including corrosiveness, competitive light absorption, and direct redox quenching of highly polarizable dyes such as conjugated porphyrins.)^{25–27} Alternatives that are demonstrably capable of regenerating dyes at lower driving force have mainly been based on one-electron redox couples. Unfortunately, concomitant with fast, low-driving-force regeneration has been fast interception of injected electrons by the oxidized form of the shuttle. One manifestation of fast interception is a greatly diminished charge-collection length, which typically results in greatly reduced DSSC efficiency. Several candidate remedies have been explored. One centers on replacing conventional ruthenium dyes with much more strongly absorbing organic dyes so that thinner photoelectrodes can be employed and shorter charge-collection lengths can be tolerated.²⁸ A second entails the introduction of physical spacers or barriers that inhibit contact between the shuttle and the electrode, thereby slowing the rate of interception.^{29–32} A third, which is the focus of the report here, would be to transport electrons more rapidly through the photoelectrode, thereby increasing the fraction of injected electrons captured and decreasing the fraction lost to interception (or to recombination with the oxidized dye). While a large number of reports exist on enhancing rates of electron transport,^{33–37} most have focused on DSSCs utilizing iodide/tri-iodide. Indeed, we are aware of no previous study where rapid electron transport has been directly examined as a strategy for enhancing the performance of DSSCs containing fast, solution-phase redox shuttles. (Evidently not yet widely appreciated is that with slow redox shuttles little can be gained by enabling faster electron transport since collection efficiencies already typically approach unity.)

As a starting point, we have focused on photoelectrodes in which, at least initially, ZnO replaces TiO₂, and in which subunits other than nanoparticles make up the photoelectrodes. Our motivation comes from several studies that indicate that transport of injected electrons through quasi-one-dimensional ZnO structures (*e.g.*, nanorods, nanowires, and nanotubes) is substantially faster than through analogous TiO₂ structures or through nanoparticulate aggregates of either material.^{34–37} The basis for faster collection is not entirely clear but has variously been attributed to larger semiconductor grain sizes,³⁸ fewer trap states (sub-band-edge electronic states),^{36,37} and/or the known higher mobility of electrons in single-crystal ZnO *versus* TiO₂.³⁹ Unfortunately, structures such as arrays of nanorods have insufficient surface area (typically *ca.* 100× geometric area) to enable enough dye loading to achieve good light harvesting. As a much higher area alternative, we have fabricated ZnO electrodes *via* atomic layer deposition (ALD) on

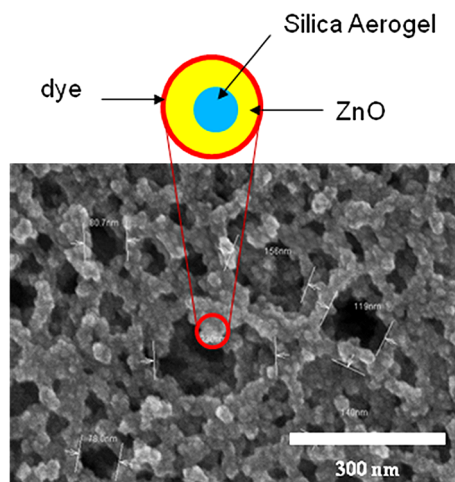


Figure 1. SEM image of SiO₂ aerogel framework coated by ALD with 10 nm ZnO.

low-density silica aerogels prepared as thin films on transparent conductive glass platforms;^{40,41} see Figure 1. An additional challenge with ZnO is its propensity to dissolve in acidic solutions, including nonaqueous solutions of weak acids such as carboxylic acids.⁴² Because dyes are typically anchored to DSSC photoelectrodes *via* pendant carboxylates, dye loading times with ZnO generally must be shortened in order to avoid either photoelectrode dissolution or the formation of multilayer dye/Zn(II) coatings (surface-precipitated coordination polymers) that are ineffectual photoelectrochemically. To circumvent this problem, we have explored here the idea of conformally coating the silica–ZnO aerogel structures with very thin layers of more robust metal oxides such as Al₂O₃, ZrO₂, or TiO₂ to create doubly coaxial structures. Our hope was to achieve high dye loading (and therefore good light harvesting) *via* noncorrosive binding to the outermost component of the core–shell–shell structures, while retaining the excellent electron transport behavior of the ZnO-based middle layer.

As detailed below, we indeed do find that doubly coaxial aerogel-based photoelectrodes (a) are stable with respect to corrosion either by acidic dyes or by basic components of the cell solution and (b) transport electrons much more rapidly than do either nanoparticulate (NP) ZnO photoelectrodes or aerogel photoelectrodes featuring only TiO₂ as the semiconducting component. Additionally, with the archetypal fast redox shuttle, ferrocenium/ferrocene, we find that the enhanced transport behavior results in greatly improved electron collection and, therefore, a 10-fold improvement in energy conversion efficiency (albeit, starting from a low absolute efficiency). Also contributing to enhanced charge collection is diminution of the rate of electron interception by the oxidized form of the redox shuttle. This desirable effect increases as the thickness of the outermost component of the coaxial structure (*i.e.*, ALD-formed TiO₂) increases.

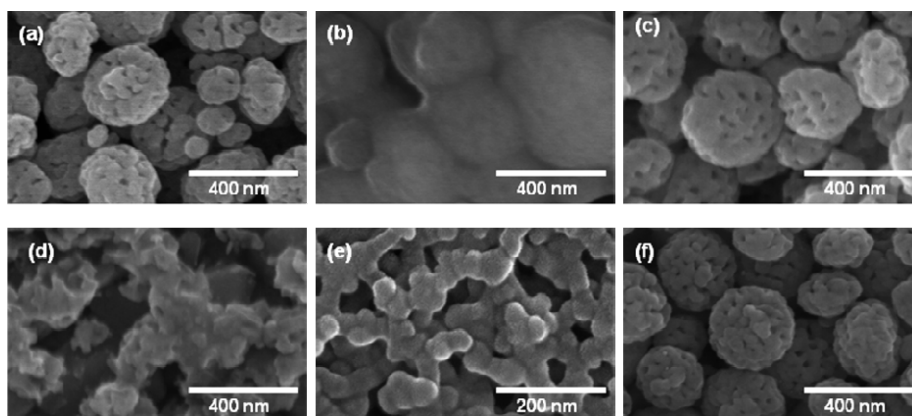


Figure 2. SEM images depicting the corrosive effects of dye solution and I^-/I_3^- electrolyte in ZnO nanoparticle films; ZnO-TiO₂ coaxial aerogel structure with protective/barrier layer; and the effect of protection from corrosion using a thin layer of TiO₂ over ZnO nanoparticles: (a) ZnO NP film dye-loaded for 30 min with no significant corrosion patterns; (b) ZnO NP film dye-loaded for 24 h showing severe corrosion defects; (c) ZnO NP film immersed in electrolyte solution after 1 day; (d) ZnO NP film immersed in electrolyte solution after 5 days; (e) no visible corrosion features on Zn-TiO₂ aerogel film after dye-loading for 24 h; (f) ZnO NP films coated (using ALD) with 10 cycles of TiO₂ and immersed in electrolyte solution after 7 days.

Finally, we find that unanticipated optical properties limit the overall energy conversion efficiencies of DSSCs containing present versions of the coaxial photoelectrodes to values less than anticipated from the observed charge-collection efficiencies.

RESULTS AND DISCUSSION

Photoelectrode Corrosion and Protection. Given the susceptibility of ZnO to corrosion even in dilute solutions of weak acids (*e.g.*, ethanol solutions of carboxylic acid functionalized dyes), we speculated that conformal ALD of an ultrathin layer of a more stable oxide could shut off this behavior. In order to visualize corrosion more easily, we substituted aggregated nanoparticulate ZnO for aerogel-templated ZnO; the former is what has most typically been used in zinc-oxide-based DSSCs. Initially we examined samples coated with a few to several angstroms of either alumina or zirconia. Consistent with the putative conformal nature of atomic-layer deposition, we observed that these structures indeed resisted corrosion by acidic dye solutions. Unfortunately, these insulating coatings also inhibited injection of electrons into ZnO by the photoexcited dye. Consequently, we turned, for most subsequent experiments, to TiO₂. N719 readily injects into this semiconductor, and the conduction-band-edge energies for TiO₂ and ZnO are likely within 0.1 eV of each other.⁴³

Figure 2 summarizes our findings. Little or no corrosion is evident after ZnO exposure to a dilute ethanolic solution of N719 for 30 min (panel a); after 24 h, however, severe corrosion has occurred (panel b). Further work (panels c and d) revealed that ZnO is also susceptible to extensive corrosion by a standard DSSC electrolyte solution also containing the weak base *tert*-butylpyridine, albeit over a period of several days; similar behavior was seen with electrolyte solutions

containing 2,6-dimethylpyridine. (*tert*-Butylpyridine is a typical additive for DSSC solutions, as it slows interception of injected electrons and may play a role in defining the energy of the conduction band edge.) As shown in panel e (note aerogel structure), treatment *via* 10 ALD cycles with TiO₂ (approximately 4 Å of TiO₂) renders zinc oxide immune to corrosion by acid dye solutions. This finding is important because, in principle, it enables the aerogel dye-loading step to be prolonged sufficiently for the resulting photoanodes to function well as light harvesters. Finally, panel e shows that treatment of ZnO with 10 cycles of ALD titanium dioxide (about 4 Å) also provides protection against corrosion caused by *tert*-butylpyridine.

Charge Transport. Electrochemical impedance spectroscopy was used to study the dynamics of charge transport and charge transfer within DSSCs,⁴⁴ with a specific focus on transport of electrons within the aerogel-based electrodes. Electrochemical impedance is a measure of the ability of a circuit to resist the flow of electrical current, and it is most easily evaluated by applying a small ac potential to an electrochemical cell and measuring the current response, as functions of both the ac frequency and the applied (dc) potential. Figure 3 shows Nyquist plots of the imaginary ($Z''(\Omega)$) versus real ($Z'(\Omega)$) components of the impedance of an aerogel-based DSSC in the absence of illumination, but with applied biases of 0.25, 0.30, and 0.35 V. The anode composition was SiO₂-ZnO-ZrO₂. At high frequencies (lower left corner of Figure 3), we observed a small arc corresponding to the charge-transfer resistance (R_{ct}) at the Pt-coated counter electrode (*i.e.*, impedance contributions associated with conversion of I_3^- back to I^-). At intermediate frequencies (see inset), we observed for each plot a 45° line characteristic of Warburg-like diffusion behavior and corresponding to transport of electrons through the aerogel electrode.

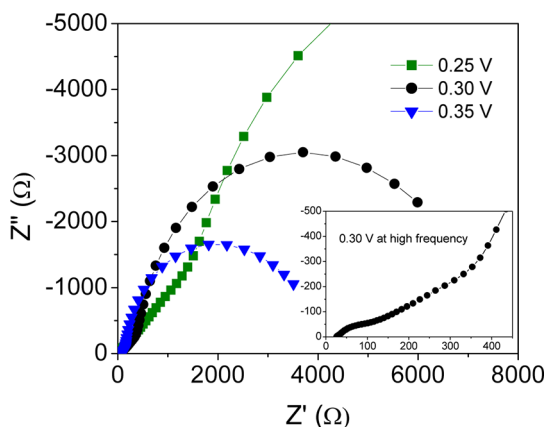


Figure 3. Nyquist plots of ZrO_2 -coated ZnO aerogel DSSC at 0.25 V (green squares), 0.3 V (black circles), and 0.35 V (blue triangles). The inset displays an enlarged spectrum of 0.3 V at high frequency to emphasize the Warburg diffusion behavior from which electron transit times are extracted.

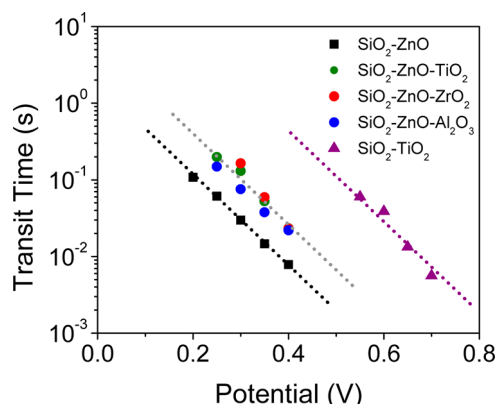


Figure 4. Comparison of the transit time of electrons injected into SiO_2 -ZnO-coated aerogel devices (squares), relative to ZnO-protected films with Al_2O_3 , ZrO_2 , and TiO_2 (circles) and also relative to SiO_2 - TiO_2 aerogel devices (triangles).

Finally, at low frequencies, we observed a larger arc assignable to electron interception by tri-iodide at the anode/solution interface, where our analyses were based on a well-established DSSC transmission-line model.^{34,45}

Figure 4 illustrates how the electron-transport dynamics varies as functions of both cell potential and aerogel anode composition. The results are presented in terms of electron transit times, τ_d . In all cases the transit times show the expected exponential decrease with increasing anode–cathode potential difference. Comparing the various electrode compositions, two observations stand out. First, consistent with other reports, τ_d values for SiO_2 -ZnO are roughly 2 orders of magnitude smaller than for SiO_2 - TiO_2 .⁴⁶ Second, electron transport within doubly coaxial photoelectrodes featuring ultrathin ALD-formed coatings of TiO_2 , ZrO_2 , or Al_2O_3 is much faster than within SiO_2 - TiO_2 electrodes, with transit times approaching those for SiO_2 -ZnO electrodes. These results strongly

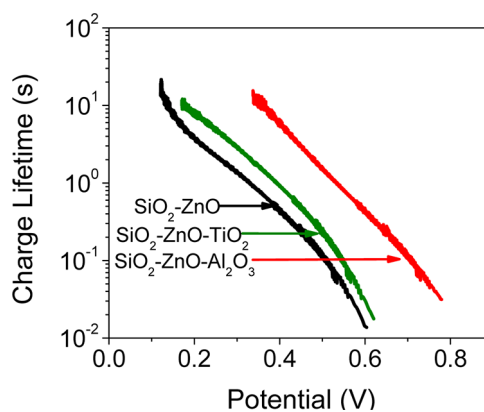


Figure 5. Charge lifetimes from open-circuit decay measurements for DSSC devices (utilizing I^-/I_3^- as the redox shuttle) made from ZnO-ALD-modified silica aerogels (black) and devices with separate overcoats of TiO_2 (green) and Al_2O_3 (red). See Table 1 for device performances.

suggest that for the doubly coaxial structures the ZnO component serves as the primary conduit for electron transport. Finally, we also examined the dependence of transit times on TiO_2 thickness. The Supporting Information (SI), Section 3, can be consulted for detailed information. Briefly, however, varying the TiO_2 thickness from ~ 0.4 nm to ~ 5.7 nm, with SiO_2 -ZnO- TiO_2 electrodes, had no effect upon transport times.

Electron Interception. To evaluate rates of interception of injected electrons by the oxidized form of the redox shuttle, open-circuit voltage decay (OCVD) measurements were made. Briefly, these entail (a) holding a cell at open circuit under constant illumination until constant voltage achieved a stationary state, (b) rapidly ending the illumination, and (c) recording the decay in complete darkness, as the electrons in the photoanode are intercepted by the oxidized form of the shuttle. The rate of decay at any particular (open-circuit) potential, V_{oc} , is related to the electron survival lifetime (*i.e.*, interception time, τ_n) at that potential *via* the following:⁴⁷

$$\tau_n = -\frac{k_B T}{e} \left(\frac{dV_{oc}}{dt} \right)^{-1}$$

where k_B is the Boltzmann constant, T is the absolute temperature, e is the unit electronic charge, and t is time. OCVD curves are simple exponential decays if the dominant interception pathway in the cell is from the thermal population of the conduction band to the redox shuttle. If there are competing interception pathways, however, the OCVD curves may deviate from simple single-exponential form.⁴⁷

Figure 5 summarizes the results, which are presented in semilogarithmic form as plots of survival times of injected electrons *versus* cell potential. Longer times are more desirable, as they translate into longer charge-collection distances and asymptotically larger photocurrents and photovoltages. Shown are plots for SiO_2 -ZnO (6 nm shell), SiO_2 -ZnO- TiO_2 (6 and 0.4 nm

shells, respectively), and $\text{SiO}_2\text{-ZnO-Al}_2\text{O}_3$ (6 and 0.3 nm shells, respectively), with I^-/I_3^- as the redox shuttle. Using devices described in Table 1, OCVD measurements were obtained, and the electron lifetimes were calculated and plotted in Figure 5. In devices coated with Al_2O_3 , the electron lifetime increases by *ca.* 7- to 10-fold (depending on potential), implying that the rate of electron interception by triiodide is slowed by *ca.* 7- to 10-fold. The dark current arising from the interception reaction was also reduced (Figure 6) and is consistent with a 173 mV increase in the photovoltage extracted from the devices when compared to the ZnO control cells. From previous studies with tin-oxide photoelectrodes, we found that conformal alumina coatings slowed electron interception both by passivating sub-band-edge surface states that are catalytic for electron interception and by imposing a tunneling barrier to back electron transfer.⁴⁸ The latter leads to an exponential falloff in electron-transfer rate with barrier layer thickness. Assuming, for the moment, that the falloff with alumina-coated ZnO is the same as with alumina-coated SnO_2 , a $1/e$ rate decrease is anticipated for each angstrom of added barrier material. Thus, a 0.3 nm alumina barrier layer would slow the rate of electron interception by roughly a factor of 12, in reasonable agreement with our observations. Thus, surface-state passivation appears not to be a significant factor in slowing interception at the $\text{SiO}_2\text{-ZnO-Al}_2\text{O}_3$ /solution interface. Unfortunately, thicker alumina layers, which should further attenuate the interception rate, also inhibit

electron injection. Indeed, from Figure 6, even a 0.3 nm layer of alumina appears to inhibit electron injection, judging by the attenuation of the photocurrent density at short circuit.

Figure 7 shows electron lifetime plots of 6 nm thick ZnO aerogel films coated with 0.4, 1.6, and 5.7 nm thick TiO_2 shells. We find that with 0.4 nm of TiO_2 , the electron lifetime increases by *ca.* 2- to 3-fold (depending on potential), while with 5.7 nm of TiO_2 it increases by *ca.* 40-fold, implying that the rate of electron interception is slowed by *ca.* 40-fold. The findings for alumina coatings appear to rule out surface-state passivation as an explanation for the large effects, as no evidence was found for the existence of ZnO surface states that are catalytic for electron injection. Given the similarity in band-edge energies for ZnO and TiO_2 —typically estimated to be within 0.1 V of each other—tunneling-based rate attenuation is likely implausible. We speculatively attribute the effects to TiO_2 band bending, which should become progressively more important as the TiO_2 layer thickness increases. While band bending generally can be neglected with nanoparticulate electrodes, the same may not be true for rod-, tube-, or cylinder-shaped electrode microstructures. Unpublished work from our lab, with

TABLE 1. Photovoltaic Parameters for a 25 μm thick $\text{SiO}_2\text{-ZnO}$ Aerogel Film-Containing DSSC, Compared to DSSCs featuring Similar Photoelectrodes, but with *ca.* 3 and 4 Å Coatings of Al_2O_3 and TiO_2 , Respectively

aerogel-based photoelectrodes	J_{sc} (mA/cm^2)	V_{oc} (V)	FF^a (%)	η (%)
$\text{SiO}_2\text{-ZnO}$	6.82	0.596	46	1.87
$\text{SiO}_2\text{-ZnO-Al}_2\text{O}_3$	4.40	0.769	49	1.66
$\text{SiO}_2\text{-ZnO-TiO}_2$	7.64	0.627	51	2.44

^a Fill factor.

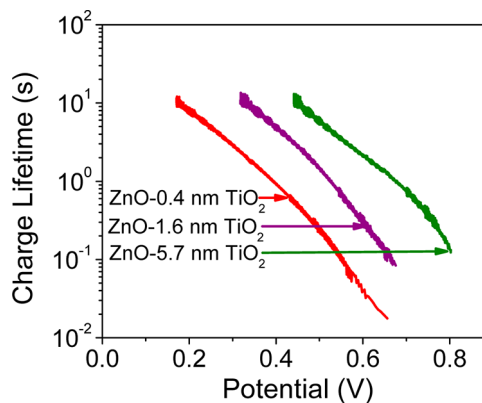
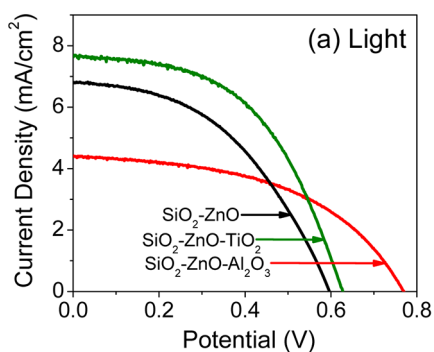


Figure 7. Plot showing the effects of increased layers of TiO_2 coats over 6 nm ZnO-coated silica aerogels with respect to charge lifetimes from OCVD measurements.

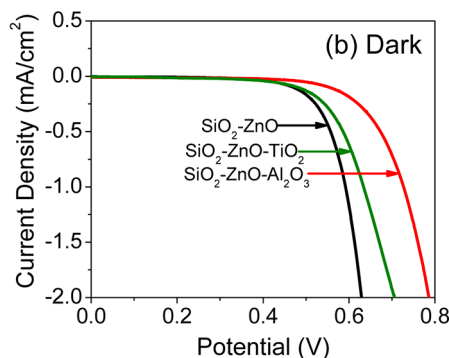


Figure 6. J - V characteristics of DSSCs featuring 25 μm thick aerogel-based $\text{SiO}_2\text{-ZnO}$ films compared to similar films with *ca.* 3 and 4 Å coatings of Al_2O_3 and TiO_2 , respectively: (a) light performance; (b) dark performance. Note: Curves correspond to the data shown in Table 1.

ALD-prepared flat TiO₂ electrodes (Mott–Schottky experiments), shows that adventitious doping is sufficient to support substantial band bending over the distances (thicknesses) encountered here (ca. 4 nm).⁴⁹

Charge Collection. Efficient charge collection is a prerequisite for efficient light-to-electrical energy conversion. Charge collection efficiencies (η_{cc}) approaching unity are expected when the effective electron diffusion length, L_n , exceeds the overall photoanode thickness, L , a condition that is met when the electron transit time, τ_d , is less than the electron interception time (electron lifetime, τ_n) or, equivalently, when R_{ct} exceeds R_{tr} . The effective electron diffusion length can be calculated from⁵⁰

$$L_n = \sqrt{D_n \tau_n} = L \sqrt{\frac{\tau_n}{\tau_d}} = L \sqrt{\frac{R_{ct}}{R_{tr}}}$$

where D_n is the diffusion coefficient for the electron within the electrode, R_{ct} is the interfacial charge-transfer resistance, and R_{tr} is the resistance associated with electron transport through the semiconductor. Using values obtained from electrochemical impedance spectroscopy (EIS), we find that L_n is ~ 200 and $\sim 300 \mu\text{m}$ for the $25 \mu\text{m}$ thick SiO₂–ZnO and SiO₂–ZnO–TiO₂ aerogel photoelectrode, respectively (see SI, Section 4). Thus, the charge-collection efficiency is essentially unity with I[−]/I₃[−] as the redox shuttle.

Overall Energy Conversion Efficiencies with I[−]/I₃[−] As the Redox Shuttle. DSSCs featuring $25 \mu\text{m}$ thick, aerogel-based SiO₂–ZnO (6 nm thick ZnO shells) photoelectrodes that had been dye-loaded for 30 min yielded superior photovoltaic parameters [$V_{oc} = 0.596 \text{ V}$, $J_{sc} = 6.82 \text{ mA/cm}^2$, FF = 46%, and $\eta = 1.87\%$] compared with similar films dye-loaded for 24 h [$V_{oc} = 0.52 \text{ V}$, $J_{sc} = 2.08 \text{ mA/cm}^2$, FF = 43%, and $\eta = 0.47\%$]. As shown in Figure 8, replacing ZnO with TiO₂ yielded modest improvements in all three parameters. We will defer discussion of the basis for the improvement until a subsequent section. It is important to appreciate, however, that when the efficiency for charge collection is high, increasing the rate of electron transport (e.g., by replacing TiO₂ with ZnO) confers no advantage in terms of overall energy conversion efficiency.

Illustrated in Figure 6, and detailed in Table 1, are the effects of elaborating the electrodes by incorporating a second shell consisting of 3 and 4 Å of Al₂O₃ and TiO₂, respectively. The former increases V_{oc} but diminishes J_{sc} , effects that are consistent respectively with diminished dark current production and reduced efficiency for electron injection (due to diminished electronic coupling between the semiconductor and the photoexcited dye). For SiO₂–ZnO–TiO₂, J_{sc} and V_{oc} both increase slightly relative to SiO₂–ZnO. The increase is tentatively ascribed to improved light harvesting, due to greater dye loading, a consequence of longer loading times. The increase in V_{oc} is consistent

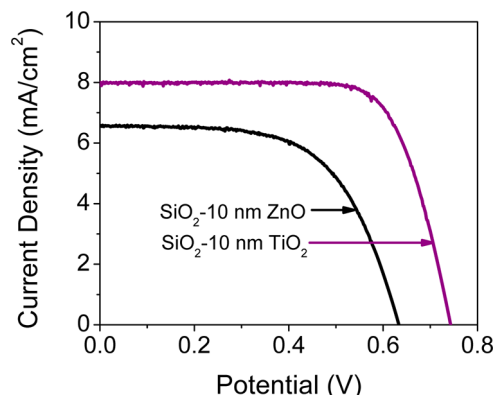


Figure 8. J – V characteristics for optimized $25 \mu\text{m}$ thick SiO₂ aerogel films, coated by ALD with 10 nm TiO₂ (purple) and 10 nm ZnO (black) and employed in DSSCs. TiO₂ DSSCs: $V_{oc} = 0.75 \text{ V}$, $J_{sc} = 7.96 \text{ mA/cm}^2$, FF = 72%, $\eta = 4.30\%$. ZnO DSSCs: $V_{oc} = 0.63 \text{ V}$, $J_{sc} = 6.57 \text{ mA/cm}^2$, FF = 61%, $\eta = 2.52\%$.

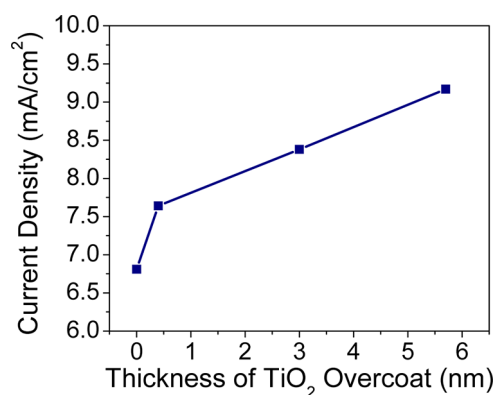


Figure 9. Plot showing an increase in J_{sc} with increased thicknesses of TiO₂ coats over SiO₂–6 nm ZnO aerogels.

with a modest decrease in dark current, as shown in Figure 6b. Illustrated in Figure 9 are the effects of systematically increasing the thickness of the TiO₂ shell, in this case starting with a silica aerogel featuring only a 6 nm shell of ZnO. The observed sizable increases in J_{sc} are likely consequences mainly of increasing light harvesting, due to increased photoelectrode surface area. (Recall that for an isolated cylindrical strand the surface area scales as the diameter of the strand.) Dye molecules were desorbed *via* immersion in 0.3 M tetrabutylammonium hydroxide–ethanol solution from a series of nominally identical SiO₂–ZnO aerogel electrodes coated with 0.4 and 5.7 nm TiO₂ in order to estimate the photoelectrode roughness. Roughness factors of 2400 and 2700 were estimated for SiO₂–ZnO–0.4 nm TiO₂ and SiO₂–ZnO–5.7 nm TiO₂, respectively.⁵¹ Estimating roughness by dye desorption excludes any part of the aerogel surface area inaccessible to dye, for example, topological features that are smaller than the dye. A possible secondary contributor may be a slight improvement in charge-collection efficiency. As shown in Figure 7, rates for electron interception decrease substantially as the thickness of TiO₂ in SiO₂–ZnO–TiO₂ structures is

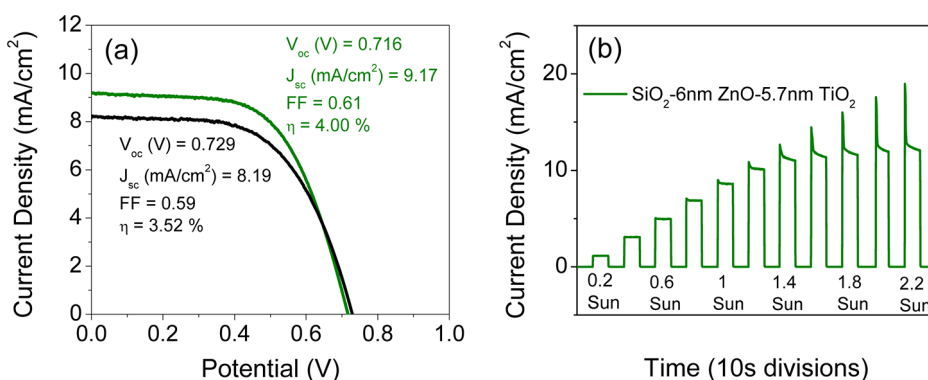


Figure 10. Plots indicating (a) optimized J - V plots for silica aerogel devices with 6 nm ZnO film coated with 5.7 nm TiO_2 (green) and 2 nm ZnO film coated with 5.7 nm TiO_2 (black), under AM 1.5 illumination, and (b) current transient data for a silica aerogel device with 6 nm ZnO and an overcoat of 5.7 nm TiO_2 .

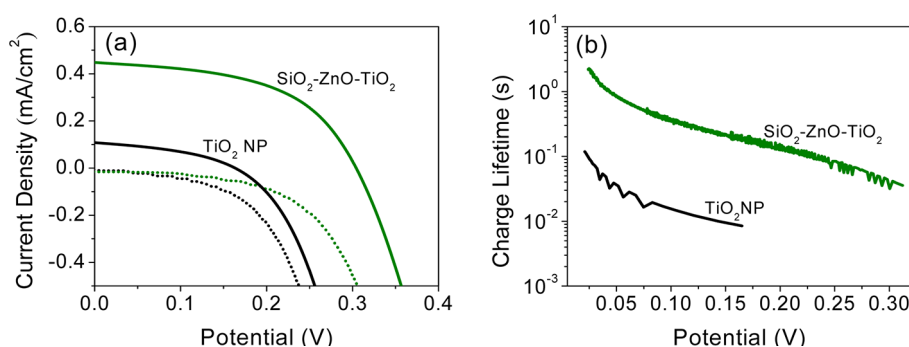


Figure 11. Photovoltaic performances of devices using the Fc/Fc^+ redox shuttle. (a) J - V characteristics for devices fabricated with SiO_2 -6 nm ZnO-5.7 nm TiO_2 aerogels and TiO_2 nanoparticle photoanodes under 1 sun illumination (solid lines) and in the dark (dotted lines). (b) Electron lifetime plots calculated from open-circuit voltage decay measurements.

increased.⁵² A seemingly similar trend has been reported for ALD-prepared coatings of TiO_2 on ZnO nanowires, but tentatively ascribed instead to greater crystallinity for thicker coatings, potentially resulting in better injection or charge transport.⁵³

With these findings in hand, several additional combinations of ZnO and TiO_2 shell thicknesses were examined, with the aim of maximizing the overall energy conversion efficiency. Ultimately, DSSCs with efficiencies of 4.0% and short-circuit current densities of 9.2 mA/cm^2 were obtained from DSSCs containing silica aerogel photoelectrodes having ZnO and TiO_2 shell thicknesses of *ca.* 6 and 5.7 nm, respectively (Figure 10a). These photoelectrodes are characterized by good dye loading, fast electron transport, slow electron interception, and efficient electron collection. It was initially surprising, therefore, that substantially higher photocurrents and efficiencies were not obtained. One possibility, not yet considered, was that J_{sc} is constrained by the rate of transport of tri-iodide through 25 μm thick aerogel coatings. Photocurrent transient experiments (Figure 10b) performed with devices containing SiO_2 -ZnO- TiO_2 anodes (5.7 nm of TiO_2) showed minimal mass transport limitation at 1 sun, indicating that some other factor must be limiting J_{sc} .⁵⁴

Overall Energy Conversion Efficiencies with Ferrocene/Ferrocenium As the Redox Shuttle. The large value of the effective charge-collection length relative to the aerogel electrode thickness, the accelerated electron transport with ZnO-containing aerogels, and the diminished rate of electron interception with the addition of TiO_2 coatings to SiO_2 -ZnO structures suggests that there is enough kinetic redundancy for faster redox shuttles to be substituted for iodide/tri-iodide without loss of charge-collection efficiency. An extreme test would be replacement of iodide/tri-iodide with ferrocene/ferrocenium. Note that we have previously observed that electron interception rates (with SiO_2 - TiO_2 electrodes) are about 5 orders of magnitude faster with ferrocenium than with tri-iodide.¹² Shown in Figure 11a is the J - V curve for an N719-sensitized cell featuring a nanoparticulate TiO_2 electrode and ferrocene/ferrocenium. Consistent with earlier work, the cell is characterized by miniscule photocurrents ($J_{\text{sc}} = 0.11 \text{ mA}/\text{cm}^2$), a small open-circuit photovoltage (166 mV), and small FF (41%). Substitution of a SiO_2 -ZnO- TiO_2 aerogel electrode (6 nm ZnO + 5.7 nm TiO_2) for the nanoparticulate electrode increases J_{sc} to 0.45 mA/cm^2 , V_{oc} to 306 mV, and FF to 52%. Taken together, these changes yield a 10-fold increase in the energy conversion efficiency.

Figure 11b shows that the increased efficiency is accompanied, as expected, by increased electron survival times. Nevertheless, the overall energy conversion efficiency is still about 60 times less, and the short-circuit current density about 20 times less, than with iodide/tri-iodide as the redox shuttle. The efficiency for electron injection should be unaffected by changing the redox shuttle. In principle, inefficient dye regeneration ($\text{Dye}^+ + \text{Fc} \rightarrow \text{Dye} + \text{Fc}^+$) could diminish photocurrents; that is, photocurrent could be lost to recombination ($\text{e}^-_{(\text{electrode})} + \text{Dye}^+ \rightarrow \text{Dye}$). Poor fill factors (observed here) are one signature of such behavior, which conceivably could arise if we have used too low a concentration of ferrocene. Nevertheless a 20-fold diminution seems too great a factor to be accounted for solely by inefficient regeneration.

A third possibility is that charge collection, while improved relative to nanoparticulate electrodes, is still inefficient due to rapid interception of injected electrons by Fc^+ . A comparison of photovoltage decay plots for cells containing Fc/Fc^+ (Figure 11b) versus I^-/I_3^- (Figure 7) shows that the combination of electron interception and electron recombination is *ca.* 4 orders of magnitude faster for the former if (extrapolated) comparisons are made at the same cell potential. This observation is broadly consistent with the *ca.* 500 mV difference in open-circuit photovoltages for the two types of cells (and essentially quantitatively consistent if the average value of the diode-quality factor is *ca.* 2 with both redox shuttles).

A test of whether faster interception also accounts for the substantial decrease in photocurrent would be to evaluate the charge-collection length in the Fc/Fc^+ , $\text{SiO}_2\text{-ZnO-TiO}_2$ cell. One way of doing this is to compare incident-photon-to-current-efficiency (IPCE) plots for front-side versus back-side illumination of the photoelectrode.⁵⁵ At wavelengths where the absorbance is high, the light-collection depth will be small and charges will mainly be generated in a narrow region of the photoelectrode closest to the light source. Thus, for back-side illumination, a large fraction of the injected electrons will be generated far from the current collector and will need to travel perhaps 20 μm or more to contribute to the photocurrent. For front-side illumination, however, injected electrons are generated close to the current collector and need to travel only a comparatively short distance to contribute to the photocurrent. Figure 12 shows IPCE plots for the two illumination geometries as well the ratio of photocurrents as a function of incident wavelength for back-side versus front-side illumination. (See SI Section 5 for discussion regarding the shapes of IPCE plots.) The findings are striking: The IPCE plots are nearly identical, indicating that current collection occurs with nearly identical efficacy for electrons injected far from the current collector versus near. Thus, interception of injected electrons by Fc^+ appears *not* to account

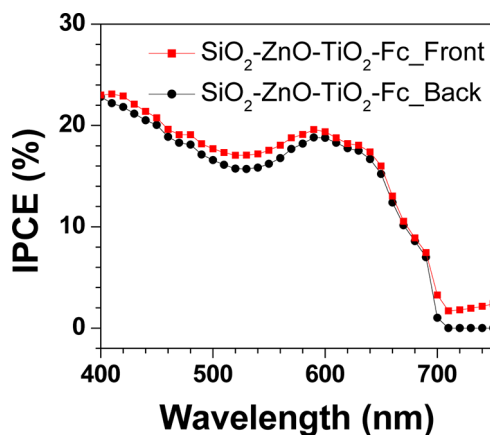


Figure 12. IPCE front-side/back-side illumination comparison of devices containing the doubly coaxial aerogel photoanode (6 nm ZnO and 5.7 nm TiO_2) using the Fc/Fc^+ redox shuttle.

for the observed 20-fold decrease in J_{sc} versus cells containing iodide/tri-iodide.

Returning to the IPCE plots, an unusual observation in view of the 25 μm thickness of the photoelectrode, the large charge-collection distances, and the previously established large surface areas of aerogel electrodes is the close similarity between both IPCE line shapes and the known absorption spectrum of N719 on TiO_2 .⁵⁶ Under these conditions, the IPCE curves should instead track the light-harvesting efficiency (LHE) of the photoelectrodes and display a much less well-defined maximum, since $\text{LHE} = 1 - 10^{-A}$, where A is the wavelength-dependent absorbance, and should have a value well above 1 over the majority of the visible spectrum. The combined results indicate that the wavelength-dependent values of the light-harvesting efficiency for the aerogel photoelectrode are much smaller than we have imagined. The likely culprit is light scattering that is efficient enough to reduce light-penetration depths, and therefore absorbances, to only small fractions of the values expected based on the high surface areas of the aerogel photoelectrodes. We have previously noted the propensity for aerogel photoelectrodes to scatter light, but did not appreciate the consequences in terms of depths of penetration.

An obvious consequence of poor light penetration is that significant numbers of electrons will be generated and significant numbers of Ru(III) species will be formed only within the first few micrometers or less of the front or back side of the photoelectrode (depending on the direction of illumination). If the primary photocurrent loss pathway is electron recombination with Ru(III), electrons should be able to travel long distances (for example, to a far-side current collector) once they have escaped the narrow region of the photoelectrode that contains significant concentrations of Ru(III). Figure 12 illustrates the idea.

Returning to cells based on iodide/tri-iodide, light loss to scattering is a plausible explanation for the

failure of J_{sc} to top 9.2 mA/cm². (Current densities of ca. 18 to 20 mA/cm² would be expected if no light were lost to scattering.) It follows that a substantial fraction of the 25 μ m photoelectrode does not effectively participate in light harvesting and could be discarded without damaging photocurrent production. Ancillary consequences of employing a thinner photoelectrode would be more effective transport of tri-iodide and a modest decrease in dark current. An improved design would employ higher extinction dyes. For cells employing ferrocene/ferrocenium, substantial performance gains should be possible by significantly increasing the rate of dye regeneration (*i.e.*, Ru(III) to Ru(II) conversion) or decreasing the rate constant for recombination of injected electrons with the oxidized form of the dye.

CONCLUSIONS

Mesoporous photoelectrodes based on doubly coaxial strands can be fabricated *via* atomic layer deposition of a few nanometers of ZnO, followed by a few nanometers of TiO₂, on silica aerogel films of ca. 25 μ m thickness. The photoelectrodes display high surface areas (ca. 2400 to 2700 \times geometric area as evidenced by dye uptake). The core–shell–shell electrodes simultaneously display the desirable fast electron-transport dynamics that characterizes silica–ZnO structures and the very good chemical stability that characterizes silica–TiO₂ structures. The quasi-one-dimensional architecture of the aerogels enables band-bending effects to be exploited to slow back electron transfer, behavior that is not possible with photoelectrodes constructed instead from zero-dimensional nanoparticles. The combination of fast transport and slow recombination yields enormous effective-charge-collection

lengths (200 μ m or more) with iodide/tri-iodide as the redox shuttle, ensuring essentially quantitative collection of charges injected within the 25 μ m thick aerogel-based photoelectrode. Given the very high electrode surface areas, the affinity of the outermost shell of the aerogel for adsorption of N719, and the high charge-collection efficiency, photocurrent densities in excess of 20 mA/cm² would be expected. Instead, they reach only about 9.2 mA/cm². The shortfall has been traced to light loss due to scattering by the photoelectrode; only the first few micrometers of the aerogel film are effectively infiltrated by photons and contribute to large harvesting. This result was unanticipated, as silica-only aerogel films are reasonably close (by eye) to full transparency. ALD of high-refractive-index metal oxide coatings, however, enhances scattering. An improved design would change the aerogel feature sizes to lengths that would not as readily scatter visible light. Fast electron transport by the core–shell–shell structure should enable good charge-collection efficiencies to be achieved even with redox shuttles capable of rapidly intercepting injected electrons. Experiments involving ferrocene/ferrocenium as the redox shuttle show that solar energy conversion efficiencies can be boosted by about a factor of 10 by incorporating ZnO as a rapid charge transporter between silica and titanium dioxide. When combined with other advances such as higher extinction dyes that physically inhibit access of shuttles to the underlying photoelectrode, thinner versions of core–shell–shell aerogel-based photoelectrodes may prove useful for exploiting fast redox shuttles in dye-sensitized solar cells that attain competitive efficiencies.

EXPERIMENTAL SECTION

Unless noted otherwise, chemicals were purchased from Sigma Aldrich and were used as received. Ferrocene was purchased from Alfa Aesar. SiO₂ alcogel films were prepared in a home-built, controlled-atmosphere chamber saturated with vapor from an equal volume solution of ethanol and water. A silica solution was prepared by diluting a prehydrolysed ethyl polysilicate solution, Silbond H-5 (Silbond Corp.), to 50% by volume with ethanol. One volume equivalent of a catalyst solution (7 mL of water, 11 mL of ethanol, and 0.371 mL of stock solution) was added slowly while stirring the silica solution to form a sol. This stock solution contained 1.852 g of NH₄F, 100 mL of water, and 18.45 mL of 30% NH₄OH. Prior to the start of gelling (typically 8 min), a desired volume of sol was drop cast onto cleaned 8 Ω /cm² fluorine-doped tin oxide (FTO) supported on 1.5 \times 1.5 cm glass squares (Hartford Glass). The resulting coating was then allowed to age in the saturated chamber for at least 1 h. Following gelation, the alcogel films were exchanged with ethanol overnight to remove excess water and subsequently dried with supercritical CO₂ to form SiO₂ aerogels. Aerogel active areas (approximately 0.08 cm²) were defined by quickly scraping the films with a razor blade. The thickness of the aerogel films as measured by profilometry (Tencor, P10) was approximately 25 μ m.

Atomic layer deposition was performed with a Savannah 100 instrument (Cambridge Nanotech Inc.), using diethylzinc (DEZ),

trimethylaluminum, titanium tetraisopropoxide (TTIP), and/or tetrakis(dimethylamido)zirconium metal sources, together with distilled water or (for TiO₂) 50% aqueous hydrogen peroxide as an oxygen source. Note that the TTIP precursor was favorable in this study because it is a liquid at room temperature and fairly inexpensive. Titanium halides have been well studied for TiO₂-ALD,^{57–60} but were undesirable, as acid byproducts are released when coating high-surface-area ZnO films, which have high sensitivity to low pH's. ZnO was grown at 150 $^{\circ}$ C using reactant exposure times of 16 and 4 s for DEZ and water, respectively, and nitrogen purge times of 30 s between exposures. The growth rate of ZnO on flat platforms, as determined by ellipsometry, was 1.56 $\text{Å}/\text{cycle}$; we assume that the growth rate on the silica filaments constituting the aerogel is identical. ZnO-coated aerogel films were annealed at 450 $^{\circ}$ C in air for 15 min to increase crystallinity. Some of these samples were further coated *via* ALD with Al₂O₃, ZrO₂, or TiO₂ to generate doubly coaxial structures (core/shell/shell structures). These secondary shells were grown at 200 $^{\circ}$ C using dosing times of 30 s for metal precursors as well as oxygen sources, with nitrogen purge times of 30 s between each type of dose. Electrodes coated with TiO₂ were subsequently annealed at 450 $^{\circ}$ C in air for 15 min. The growth rates for alumina, titania, and zirconia were 1.1, 0.40, and 0.96 $\text{Å}/\text{cycle}$, respectively. Nanoparticulate ZnO electrodes were fabricated according to a previously published procedure,⁶¹

and nanoparticulate TiO₂ electrodes were fabricated from an in-house procedure previously published.⁶²

Photoelectrodes were thermally equilibrated in an oven at 85 °C and then removed and rapidly immersed in a 0.5 mM [Ru(4,4'-dicarboxy-2,2'-bipyridine)₂(NCS)₂] (N719, Dyesol) solution made with equal volumes of acetonitrile and *tert*-butanol. After 24 h, the electrodes were rinsed with acetonitrile and dried under flowing nitrogen. (In a few instances, noted below, shorter soaking times were used.) A platinized cathode, 2.5 × 2.5 cm FTO squares (15 Ω/cm² glass, Hartford Glass), was combined in a sandwich fashion with the sensitized electrode by using a 50 μm Surlyn frame and light pressure at 140 °C. A solution of 0.6 M 1-butyl-3-methylimidazolium iodide (TCI America), 0.03 M I₂, 0.1 M guanidinium thiocyanate, and 0.5 M 4-*tert*-butylpyridine in acetonitrile:valeronitrile (85:15) was introduced into each cell by vacuum filling through a hole in the cathode. For devices in which the ferrocene (Fc)/ferrocenium (Fc⁺) shuttle was employed, acetonitrile solutions containing 0.1 M Fc, 0.01 M Fc⁺, and 0.2 M tetrabutylammonium tetrafluoroborate, TBABF₄, were deoxygenated by bubbling with nitrogen, then introduced into the devices and examined immediately. An additional layer of Surlyn and glass coverslip sealed the electrolyte in the cell. Electrical contacts were made to each electrode using silver epoxy (Chemtronics) to attach tinned copper wire to each side of the photoelectrodes.

The photovoltaic properties of the cells were measured by a CH Instrument 1202 potentiostat using simulated AM 1.5 sun-light illumination, initially thought to have an intensity of 1 sun (100 mW/cm²). After all experiments had been completed and the initial version of this report had been submitted for review, we discovered a lamp calibration error.⁶³ Thus, measurements thought to have been made at 1 sun instead had been made at 1.3 sun. To facilitate comparison with results obtained in other studies and other laboratories at an intensity of 1 sun, measured current densities were adjusted downward by a factor of 1.3 (Figures 6–12, Table 1, and text). Reported device efficiencies include the 1/1.3 correction. Not taken into account are effects upon V_{oc}, since we lack the experimental information needed to attempt adjustments. The effects almost certainly are small (perhaps a few tens of millivolts). Nevertheless, the reported cell efficiencies could be slightly higher than the true efficiencies.

All cells were illuminated through an Oriol 81092 filter using the Xe lamp in a Jobin Yvon fluorimeter. Scanning electron microscopy (SEM) images were collected on a Hitachi S-4800-II cFEG SEM, where electrodes were sputtered with Au/Pd prior to image capture with an accelerating voltage of 10 kV. Electrochemical impedance spectroscopy was performed using a 1286 potentiostat (Solartron) coupled to a 1260A frequency response analyzer (Solartron) and collected over a frequency range of 0.05–500 000 Hz. Bias potentials (two-electrode cells) ranged between 100 and 800 mV, depending on the corresponding open-circuit photovoltage of the cell under illumination at 1 sun. Films were also characterized *via* powder X-ray diffraction measurements (see SI Section 1). These measurements were made by using a Rigaku XDS 2000 diffractometer featuring nickel-filtered Cu K α radiation ($\lambda = 1.5418 \text{ \AA}$). Data were collected over a range of 15° < 2 θ < 60° in 0.05° steps with a 2 s counting time per step. Samples were mounted in the window of an aluminum holder *via* double-sided tape. X-ray photoelectron spectroscopy (XPS) was performed on TiO₂-coated ZnO films to confirm the presence of the TiO₂ shell (SI Section 2). XPS measurements were made by using an Omnicron ESCA probe with Al K α radiation at an energy of 14 kV. Spectra were referenced to the C 1s peak at 284.7 eV.

Conflict of Interest: The authors declare no competing financial interest.

Acknowledgment. We thank Dr. Stacey Standridge (formerly of Northwestern) for obtaining XPS data. We thank Dr. Jeff Elam, Dr. Angel Yanguas-Gil, and Dr. Alex Martinson (Argonne National Laboratory) and Dr. Tina Li (formerly of Northwestern) for helpful discussions. SEM and XPS measurements were performed in the EPIC and KECK-II facilities of the NUANCE Center at Northwestern University. The NUANCE Center is supported by NSF-NSEC, NSF-MRSEC, the Keck Foundation, the State of Illinois, and

Northwestern University. We gratefully acknowledge financial support from the ANSER Center, an Energy Frontier Research Center funded by the U.S. Department of Energy, Office of Science, Office of Basic Energy Sciences, under Award No. DE-SC0001059. V.O.W. acknowledges a fellowship from the Initiative for Sustainability and Energy at Northwestern (ISEN), and C.P. acknowledges funding from the Strategic Fellowships for Frontier Research Networks from the Commission of Higher Education, Thailand.

Supporting Information Available: XRD and XPS spectra on film characterization of ZnO–TiO₂ aerogel films; transit time of electrons through the SiO₂–ZnO aerogel framework with an overcoat of 5.7 nm TiO₂ relative to an aerogel anode with either SiO₂–TiO₂ or SiO₂–ZnO; the diffusion length in completed devices with the SiO₂–ZnO and SiO₂–ZnO–TiO₂ aerogel architecture; explanations of the simulation of LHE for highly opaque aerogel photoelectrode. This material is available free of charge *via* the Internet at <http://pubs.acs.org>.

REFERENCES AND NOTES

- Grätzel, M. Photoelectrochemical Cells. *Nature* **2001**, *414*, 338–344.
- Hagfeldt, A.; Grätzel, M. Molecular Photovoltaics. *Acc. Chem. Res.* **2000**, *33*, 269–277.
- O'Regan, B. C.; Durrant, J. R. Kinetic and Energetic Paradigms for Dye-Sensitized Solar Cells: Moving from the Ideal to the Real. *Acc. Chem. Res.* **2009**, *42*, 1799–1808.
- Hardin, B. E.; Snaith, H. J.; McGehee, M. D. The Renaissance of Dye-Sensitized Solar Cells. *Nat. Photon.* **2012**, *6*, 162–169.
- Peter, L. M. The Grätzel Cell: Where Next? *J. Phys. Chem. Lett.* **2011**, *2*, 1861–1867.
- Meyer, G. J. The 2010 Millennium Technology Grand Prize: Dye-Sensitized Solar Cells. *ACS Nano* **2010**, *4*, 4337–4343.
- O'Regan, B.; Grätzel, M., A Low-Cost, High-Efficiency Solar Cell Based on Dye-Sensitized Colloidal TiO₂ Films. *Nature* **1991**, *353*, 737–740.
- Robertson, N. Optimizing Dyes for Dye-Sensitized Solar Cells. *Angew. Chem., Int. Ed.* **2006**, *45*, 2338–2345.
- Yella, A.; Lee, H.-W.; Tsao, H. N.; Yi, C.; Chandiran, A. K.; Nazeeruddin, M. K.; Diau, E. W.-G.; Yeh, C.-Y.; Zakeeruddin, S. M.; Grätzel, M. Porphyrin-Sensitized Solar Cells with Cobalt (II/III)-Based Redox Electrolyte Exceed 12% Efficiency. *Science* **2011**, *334*, 629–634.
- Hamann, T. W.; Jensen, R. A.; Martinson, A. B. F.; Ryswyk, H. V.; Hupp, J. T. Advancing Beyond Current Generation Dye-Sensitized Solar Cells. *Energy Environ. Sci.* **2008**, *1*, 66–78.
- Snaith, H. J. Estimating the Maximum Attainable Efficiency in Dye-Sensitized Solar Cells. *Adv. Funct. Mater.* **2010**, *20*, 13–19.
- Li, T. C.; Spokoyny, A. M.; She, C.; Farha, O. K.; Mirkin, C. A.; Marks, T. J.; Hupp, J. T. Ni(III)/(IV) Bis(dicarbollide) as a Fast, Noncorrosive Redox Shuttle for Dye-Sensitized Solar Cells. *J. Am. Chem. Soc.* **2010**, *132*, 4580–4582.
- Feldt, S. M.; Gibson, E. A.; Gabrielson, E.; Sun, L.; Boschloo, G.; Hagfeldt, A. Design of Organic Dyes and Cobalt Polypyridine Redox Mediators for High-Efficiency Dye-Sensitized Solar Cells. *J. Am. Chem. Soc.* **2010**, *132*, 16714–16724.
- Daeneke, T.; Kwon, T.-H.; Holmes, A. B.; Duffy, N. W.; Bach, U.; Spiccia, L. High-Efficiency Dye-Sensitized Solar Cells with Ferrocene-Based Electrolytes. *Nat. Chem.* **2011**, *3*, 211–215.
- Burschka, J.; Brault, V.; Ahmad, S.; Breaux, L.; Nazeeruddin, M. K.; Marsan, B.; Zakeeruddin, S. M.; Grätzel, M. Influence of the Counter Electrode on the Photovoltaic Performance of Dye-Sensitized Solar Cells Using a Disulfide/Thiolate Redox Electrolyte. *Energy Environ. Sci.* **2012**, *5*, 6089–6097.
- Hamann, T. W. The End of Iodide? Cobalt Complex Redox Shuttles in DSSCs. *Dalton Trans.* **2012**, *41*, 3111–3115.
- Hamann, T. W.; Farha, O. K.; Hupp, J. T. Outer-Sphere Redox Couples as Shuttles in Dye-Sensitized Solar Cells. Performance Enhancement Based on Photoelectrode Modification

- via Atomic Layer Deposition. *J. Phys. Chem. C* **2008**, *112*, 19756–19764.
18. Ondersma, J. W.; Hamann, T. W. Impedance Investigation of Dye-Sensitized Solar Cells Employing Outer-Sphere Redox Shuttles. *J. Phys. Chem. C* **2009**, *114*, 638–645.
 19. Hamann, T. W.; Ondersma, J. W. Dye-Sensitized Solar Cell Redox Shuttles. *Energy Environ. Sci.* **2011**, *4*, 370–381.
 20. DeVries, M. J.; Pellin, M. J.; Hupp, J. T. Dye-Sensitized Solar Cells: Driving-Force Effects on Electron Recombination Dynamics with Cobalt-Based Shuttles. *Langmuir* **2010**, *26*, 9082–9087.
 21. Sapp, S. A.; Elliott, C. M.; Contado, C.; Caramori, S.; Bignozzi, C. A. Substituted Polypyridine Complexes of Cobalt(II/III) as Efficient Electron-Transfer Mediators in Dye-Sensitized Solar Cells. *J. Am. Chem. Soc.* **2002**, *124*, 11215–11222.
 22. Bai, Y.; Yu, Q.; Cai, N.; Wang, Y.; Zhang, M.; Wang, P. High-Efficiency Organic Dye-Sensitized Mesoscopic Solar Cells with a Copper Redox Shuttle. *Chem. Commun.* **2011**, *47*, 4376–4378.
 23. Elliott, C. M. Dye-Sensitized Solar Cells: Out with Both Baby and Bathwater. *Nat. Chem.* **2011**, *3*, 188–189.
 24. Teng, C.; Yang, X.; Li, S.; Cheng, M.; Hagfeldt, A.; Wu, L.-z.; Sun, L. Tuning the HOMO Energy Levels of Organic Dyes for Dye-Sensitized Solar Cells Based on Br⁻/Br₃⁻ Electrolytes. *Chem.—Eur. J.* **2010**, *16*, 13127–13138.
 25. Boschloo, G.; Hagfeldt, A. Characteristics of the Iodide/Tri-iodide Redox Mediator in Dye-Sensitized Solar Cells. *Acc. Chem. Res.* **2009**, *42*, 1819–1826.
 26. Standridge, S. D.; Schatz, G. C.; Hupp, J. T. Toward Plasmonic Solar Cells: Protection of Silver Nanoparticles via Atomic Layer Deposition of TiO₂. *Langmuir* **2009**, *25*, 2596–2600.
 27. Splan, K. E.; Massari, A. M.; Hupp, J. T. A Porous Multilayer Dye-Based Photoelectrochemical Cell That Unexpectedly Runs in Reverse. *J. Phys. Chem. B* **2004**, *108*, 4111–4115.
 28. Page, M.; Niitsoo, O.; Itzhak, Y.; Cahen, D.; Hodes, G. Copper Sulfide as a Light Absorber in Wet-Chemical Synthesized Extremely Thin Absorber (ETA) Solar Cells. *Energy Environ. Sci.* **2009**, *2*, 220–223.
 29. Palomares, E.; Clifford, J. N.; Haque, S. A.; Lutz, T.; Durrant, J. R. Control of Charge Recombination Dynamics in Dye Sensitized Solar Cells by the Use of Conformally Deposited Metal Oxide Blocking Layers. *J. Am. Chem. Soc.* **2003**, *125*, 475–482.
 30. Clifford, J. N.; Yahioglu, G.; Milgrom, L. R.; Durrant, J. R. Molecular Control of Recombination Dynamics in Dye Sensitized Nanocrystalline TiO₂ Films. *Chem. Commun.* **2002**, 1260–1261.
 31. Handa, S.; Haque, S. A.; Durrant, J. R. Saccharide Blocking Layers in Solid State Dye Sensitized Solar Cells. *Adv. Funct. Mater.* **2007**, *17*, 2878–2883.
 32. Kay, A.; Grätzel, M. Dye-Sensitized Core–Shell Nanocrystals: Improved Efficiency of Mesoporous Tin Oxide Electrodes Coated with a Thin Layer of an Insulating Oxide. *Chem. Mater.* **2002**, *14*, 2930–2935.
 33. Galoppini, E.; Rochford, J.; Chen, H.; Saraf, G.; Lu, Y.; Hagfeldt, A.; Boschloo, G. Fast Electron Transport in Metal Organic Vapor Deposition Grown Dye-Sensitized ZnO Nanorod Solar Cells. *J. Phys. Chem. B* **2006**, *110*, 16159–16161.
 34. Martinson, A. B. F.; Góes, M. S.; Fabregat-Santiago, F.; Bisquert, J.; Pellin, M. J.; Hupp, J. T. Electron Transport in Dye-Sensitized Solar Cells Based on ZnO Nanotubes: Evidence for Highly Efficient Charge Collection and Exceptionally Rapid Dynamics. *J. Phys. Chem. A* **2009**, *113*, 4015–4021.
 35. Martinson, A. B. F.; Elam, J. W.; Hupp, J. T.; Pellin, M. J. ZnO Nanotube Based Dye-Sensitized Solar Cells. *Nano Lett.* **2007**, *7*, 2183–2187.
 36. Martinson, A. B. F.; McGarrah, J. E.; Parpia, M. O. K.; Hupp, J. T. Dynamics of Charge Transport and Recombination in ZnO Nanorod Array Dye-Sensitized Solar Cells. *Phys. Chem. Chem. Phys.* **2006**, *8*, 4655–4659.
 37. Law, M.; Greene, L. E.; Johnson, J. C.; Saykally, R.; Yang, P. Nanowire Dye-Sensitized Solar Cells. *Nat. Mater.* **2005**, *4*, 455–459.
 38. Gonzalez-Valls, I.; Lira-Cantu, M. Vertically-Aligned Nanostructures of ZnO for Excitonic Solar Cells: a Review. *Energy Environ. Sci.* **2009**, *2*, 19–34.
 39. Dittrich, T.; Lebedev, E. A.; Weidmann, J. Electron Drift Mobility in Porous TiO₂ (Anatase). *Phys. Status Solidi A* **1998**, *165*, R5–R6.
 40. Hamann, T. W.; Martinson, A. B. F.; Elam, J. W.; Pellin, M. J.; Hupp, J. T. Aerogel Templated ZnO Dye-Sensitized Solar Cells. *Adv. Mater.* **2008**, *20*, 1560–1564.
 41. Hamann, T. W.; Martinson, A. B. F.; Elam, J. W.; Pellin, M. J.; Hupp, J. T. Atomic Layer Deposition of TiO₂ on Aerogel Templates: New Photoanodes for Dye-Sensitized Solar Cells. *J. Phys. Chem. C* **2008**, *112*, 10303–10307.
 42. Keis, K.; Magnusson, E.; Lindström, H.; Lindquist, S.-E.; Hagfeldt, A. A 5% Efficient Photoelectrochemical Solar Cell Based on Nanostructured ZnO Electrodes. *Sol. Energy Mater. Sol. Cells* **2002**, *73*, 51–58.
 43. Zhang, Q.; Dandeneau, C. S.; Zhou, X.; Cao, G. ZnO Nanostructures for Dye-Sensitized Solar Cells. *Adv. Mater.* **2009**, *21*, 4087–4108.
 44. Kalyanasundaram, K. *Dye-Sensitized Solar Cell*, 1st ed.; EPFL Press: Lausanne: Switzerland, 2010.
 45. Wang, Q.; Ito, S.; Grätzel, M.; Fabregat-Santiago, F.; Mora-Sero, I.; Bisquert, J.; Bessho, T.; Imai, H. Characteristics of High Efficiency Dye-Sensitized Solar Cells. *J. Phys. Chem. B* **2006**, *110*, 25210–25221.
 46. (a) The thicknesses between the SiO₂–ZnO and SiO₂–TiO₂ aerogel photoanodes differ by 10 μm (15 μm SiO₂–TiO₂ device), so the electron transport distance is almost 2 times longer for the ZnO devices. Thus, we expect good charge-collection efficiency (η_{cc}) in these devices where good η_{cc} in DSSCs is necessary for good performances. (b) Thin-film SiO₂–ZnO aerogel structures were also found to transport electrons at least two orders of magnitude faster than a traditional TiO₂ nanoparticle framework; see: Martinson, A. B. F.; Góes, M. S.; Fabregat-Santiago, F.; Bisquert, J.; Pellin, M. J.; Hupp, J. T. Electron Transport in Dye-Sensitized Solar Cells Based on ZnO Nanotubes: Evidence for Highly Efficient Charge Collection and Exceptionally Rapid Dynamics. *J. Phys. Chem. A* **2009**, *113*, 4015–4021.
 47. Zaban, A.; Greenshtein, M.; Bisquert, J. Determination of the Electron Lifetime in Nanocrystalline Dye Solar Cells by Open-Circuit Voltage Decay Measurements. *Chem-PhysChem* **2003**, *4*, 859–864.
 48. Prasittichai, C.; Hupp, J. T. Surface Modification of SnO₂ Photoelectrodes in Dye-Sensitized Solar Cells: Significant Improvements in Photovoltage via Al₂O₃ Atomic Layer Deposition. *J. Phys. Chem. Lett.* **2010**, *1*, 1611–1615.
 49. In the absence of intentionally added dopants, TiO₂ is an n-type semiconductor with spontaneous doping attributable to oxygen vacancies. When a doped semiconductor is placed in contact with a solution containing both halves of a redox couple, the semiconductor will equilibrate electronically (*i.e.*, match its Fermi level to the Nernst potential of the redox couple) by bending its bands. The thickness of the space-charge layer depends on the concentration of dopants. Unpublished work with ALD-prepared flat electrodes yields space-charge layer thicknesses of only several nm. For an n-type semiconductor, band bending and concomitant space-charge layer formation will serve to move added electrons toward the interior of the semiconductor and away from the solution interface. The degree of band bending, as measured by a potential drop across the space-charge layer, is light-intensity dependent. At higher intensities (*i.e.*, when more electrons are being injected by photoexcited dye molecules), band bending diminishes. For conduction-band electrons to move from the semiconductor interior to the solution interface, the unfavorable potential associated with band bending must be overcome. At 298 K, every 59 mV of band bending will diminish the concentration of conduction-band electrons at the semiconductor/solution interface, relative to the semiconductor interior, by a factor of 10. If attributed entirely to band bending, the observed 40-fold

- decrease in rate of electron interception following construction of a 5.7 nm thick TiO₂ coating would require a 95 mV potential drop across the TiO₂ space-charge layer. The smaller rate effects seen with thinner coatings point to smaller potential drops and imply that these coatings are too thin to accommodate a fully formed space-charge layer.
50. Bisquert, J. Theory of the Impedance of Electron Diffusion and Recombination in a Thin Layer. *J. Phys. Chem. B* **2002**, *106*, 325–333.
 51. Assuming the dye, with a diameter of 1.4 nm, occupies an area of 1.5×10^{-14} cm², a flat electrode of area 0.67 cm² can therefore accommodate 4.0×10^{13} dye molecules. For SiO₂–ZnO–0.4 nm TiO₂: The absorbance from the dye desorbed by 3 mL of 0.3 M TBAOH was 0.067 at 518.1 nm. The N719 extinction coefficient at 518.1 nm is 2.2×10^4 L mol⁻¹ (and $b = 0.40$ cm); thus an absorbance of 0.0670 indicates a concentration of 7.5761×10^{-6} M, or 9.59×10^{16} dye molecules within a film area of 0.1427 cm². The roughness is thus 2397. For SiO₂–ZnO–5.7 nm TiO₂: The absorbance from the dye desorbed by 3 mL of 0.3 M TBAOH was 0.083 at 518.1 nm. Thus an absorbance of 0.083 indicates a concentration of 9.4×10^{-6} M, or 1.1×10^{17} dye molecules within a film area of 0.16 cm². The roughness is thus 2689.
 52. ZnO ALD-modified aerogel electrodes were also fabricated with a coating of TiO₂ (0.8 nm) followed by a coating of Al₂O₃ (1 cycle, corresponding to *ca.* half a monolayer), resulting in a core–triple shell structure. The partial alumina shell was intended to passivate/repair defects on the TiO₂ surface that may be catalytic for back electron transfer to tri-iodide, an effect that we have previously described for nanoparticulate photoelectrodes; see: DeVries, M. J.; Pellin, M. J.; Hupp, J. T. Dye-Sensitized Solar Cells: Driving-Force Effects on Electron Recombination Dynamics with Cobalt-Based Shuttles. *Langmuir* **2010**, *26*, 9082–9087. To our surprise, no improvement was observed. Instead, the following photovoltaic parameters were obtained: $V_{oc} = 0.57$ V, $J_{sc} = 6.72$ mA/cm², FF = 50%, and $\eta = 1.91\%$. The lack of improvement suggests a comparative paucity of catalytic defect sites for ALD-prepared titania *versus* nanoparticulate TiO₂.
 53. Law, M.; Greene, L. E.; Radenovic, A.; Kuykendall, T.; Liphardt, J.; Yang, P. ZnO–Al₂O₃ and ZnO–TiO₂ Core-Shell Nanowire Dye-Sensitized Solar Cells. *J. Phys. Chem. B* **2006**, *110*, 22652–22663.
 54. At higher light intensities, however, initial illumination is accompanied by a burst of photocurrent that is not fully sustainable, implying that a higher tri-iodide concentration will be needed if a cell is operated above 1 sun. One consequence of increasing the tri-iodide concentration would be a proportional increase in dark current and a slight decrease in open-circuit photovoltage.
 55. Barnes, P. R. F.; O'Regan, B. C. Electron Recombination Kinetics and the Analysis of Collection Efficiency and Diffusion Length Measurements in Dye Sensitized Solar Cells. *J. Phys. Chem. C* **2010**, *114*, 19134–19140.
 56. Attempts to measure directly the absorbance of N719 on aerogel photoelectrodes were thwarted by excessive light scattering, even when an integrating sphere was employed.
 57. Lakomaa, E. L.; Haukka, S.; Suntola, T. Atomic Layer Growth of TiO₂ on Silica. *Appl. Surf. Sci.* **1992**, *60–61*, 742–748.
 58. Aarik, J.; Aidla, A.; Uustare, T.; Kukli, K.; Sammelselg, V.; Ritala, M.; Leskelä, M. Atomic Layer Deposition of TiO₂ Thin Films from TiI₄ and H₂O. *Appl. Surf. Sci.* **2002**, *193*, 277–286.
 59. Ritala, M.; Leskelä, M.; Nykänen, E.; Soininen, P.; Niinistö, L. Growth of Titanium Dioxide Thin Films by Atomic Layer Epitaxy. *Thin Solid Films* **1993**, *225*, 288–295.
 60. Ferguson, J. D.; Yoder, A. R.; Weimer, A. W.; George, S. M. TiO₂ Atomic Layer Deposition on ZrO₂ Particles using Alternating Exposures of TiCl₄ and H₂O. *Appl. Surf. Sci.* **2004**, *226*, 393–404.
 61. Chou, T. P.; Zhang, Q.; Fryxell, G. E.; Cao, G. Z. Hierarchically Structured ZnO Film for Dye-Sensitized Solar Cells with Enhanced Energy Conversion Efficiency. *Adv. Mater.* **2007**, *19*, 2588–2592.
 62. Jeong, N. C.; Farha, O. K.; Hupp, J. T. A Convenient Route to High Area, Nanoparticulate TiO₂ Photoelectrodes Suitable for High-Efficiency Energy Conversion in Dye-Sensitized Solar Cells. *Langmuir* **2011**, *27*, 1996–1999.
 63. Son, H.-J.; Wang, X.; Prasittichai, C.; Jeong, N. C.; Aaltonen, T.; Gordon, R. G.; Hupp, J. T. Glass-Encapsulated Light Harvesters: More Efficient Dye-Sensitized Solar Cells by Deposition of Self-Aligned, Conformal, and Self-Limited Silica Layers. *J. Am. Chem. Soc.* **2012**, *134*, 9537–9540.